Check for updates

Three-dimensional reduced graphene oxide decorated with cobalt metaphosphate as high cost-efficiency electrocatalysts for the hydrogen evolution reaction†

Zijie Tang, [ab] Shenqi Wei, [ab] Yuanyuan Wang [ID] *[ab] and Liyi Dai *[ab]

The development of cost-effective non-noble metal electrocatalysts is critical for the research of renewable energy. Transition metal cobalt metaphosphate-based materials have the potential to replace the noble metal Pt. Hence, in this work, we synthesize three-dimensional graphene-supported cobalt metaphosphate ($Co(PO_3)_2$-3D RGO) for the first time through the one-step hydrothermal synthesis method at low temperature with the aid of PH_3 phosphating. In a 0.5 mol L^{-1} H_2SO_4 solution, the obtained electrocatalyst exhibits excellent electrochemical activity for the hydrogen evolution reaction (HER) with a small overpotential of 176 mV at a current density of 10 mA cm^{-2} and a Tafel slope of 63 mV dec^{-1}. Additionally, in a 1 mol L^{-1} KOH solution, the electrocatalyst also shows outstanding HER activity with a small overpotential of 158 mV at a current density of 10 mA cm^{-2} and a Tafel slope of 88 mV dec^{-1}. $Co(PO_3)_2$-3D RGO can maintain its catalytic activity for at least ten hours whether in acid or alkali. This work not only demonstrates an excellent electrocatalyst for the hydrogen evolution reaction, but also provides an extremely convenient preparation technology, which provides a new strategy for the development and utilization of high-performance electrocatalysts.

Introduction

With the rapid development of economy and the improvement of people's living standards, there has been a large amount of energy consumption, which has led to various crises such as global environmental pollution, energy crisis, and global warming. It is extremely urgent to develop new energy to replace the exhaustible fossil fuels. Hydrogen has been widely studied as a substitute for fossil fuels.[1–3] It has the advantages of zero carbon emissions, high energy density, and abundant sources, and has become the ideal future energy.[4–7] Electrochemical water splitting has broad application prospects in the field of large-scale water splitting, which has attracted extensive attention from researchers.[5–7,13] At present, platinum-based catalysts are considered to be extremely excellent HER catalysts, but their high cost, narrow application range, and platinum's scarcity immensely restrict the extensive use of hydrogen-related technologies. Therefore, it is urgent to develop a low-cost and easily available non-noble metal catalyst to replace platinum-based catalysts.[11–13]

In recent years, transition metals have been broadly used for electrocatalytic water splitting and proved to be a very prospective HER material. Transition metal electrocatalysts can be roughly divided into the following categories: metal phosphides,[5,6,8,10–12,14] metal carbides,[15] metal nitrides,[16,17] metal sulfides,[9] metal selenides[18] and metal borides,[19] etc. Cobalt-based phosphide in HER has a great deal of attention, in which HER properties of cobalt phosphide have been extensively studied.[5,10,20–23] These cobalt phosphide compounds due to their poor electrical conductivity can only achieve a good result for HER in specific electrolyte, but they can't reach a satisfactory level. At the same time, cobalt metaphosphate-based materials (including cobalt metaphosphate and cobalt sodium metaphosphate) have been widely used in energy-related fields such as batteries due to their cheapness, cleanliness, ease of preparation, and favorable physical and chemical properties.[24–27] In recent years, researchers have discovered that different cobalt phosphate materials can be used not only in energy fields such as batteries, but also as high-efficiency electrocatalysts for oxygen evolution reactions, in which phosphate groups can accept protons and accelerate the adsorption of water molecules.[25,28–31] Considering the high activity of the cobalt-based catalyst center for HER and the advantages of the phosphoric acid group, we choose to study the hydrogen evolution ability of the cobalt phosphate-based electrocatalyst. However, there are still some challenges, including low

[a]College of Chemistry and Molecular Engineering, East China Normal University, No. 500 Dongchuan Road, Shanghai, 200241, P. R. China. E-mail: ecnu_yywang@163.com
[b]Shanghai Key Laboratory of Green Chemistry and Chemical Processes, East China Normal University, Shanghai, 200062, P. R. China

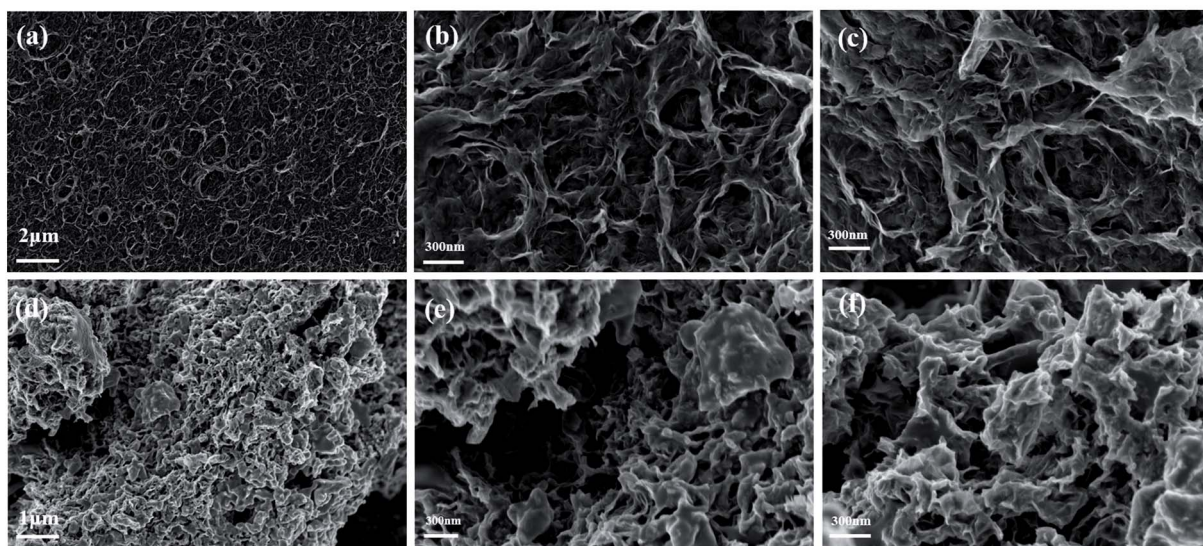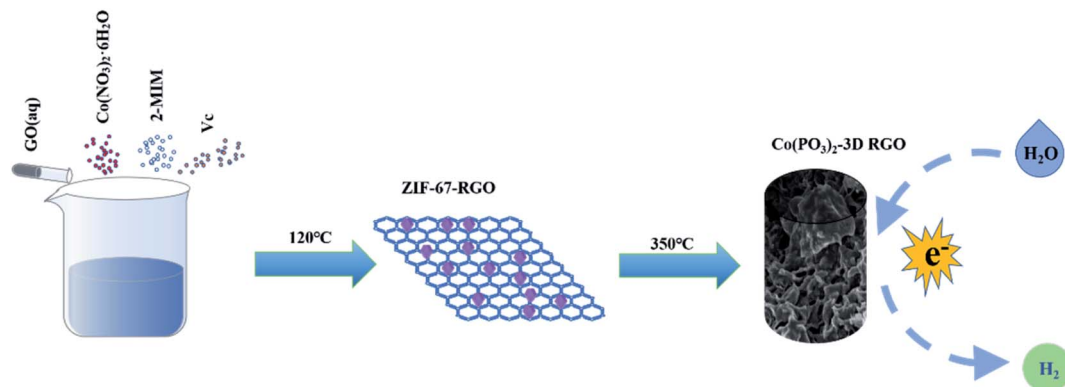† Electronic supplementary information (ESI) available. See DOI: 10.1039/d2ra01271e

Fig. 1 (a–c) SEM images of 3D RGO, (d–f) SEM images of $Co(PO_3)_2$-3D RGO.

conductivity, stability and the tendency of the catalyst to aggregate, which may result in too little exposure of the active site and too weak electron transfer ability.[7] Therefore, hunting for a supporter with good conductivity and stability is crucial to exert the highly active hydrogen evolution capacity of the cobalt phosphate material. Among them, carbon materials are ideal
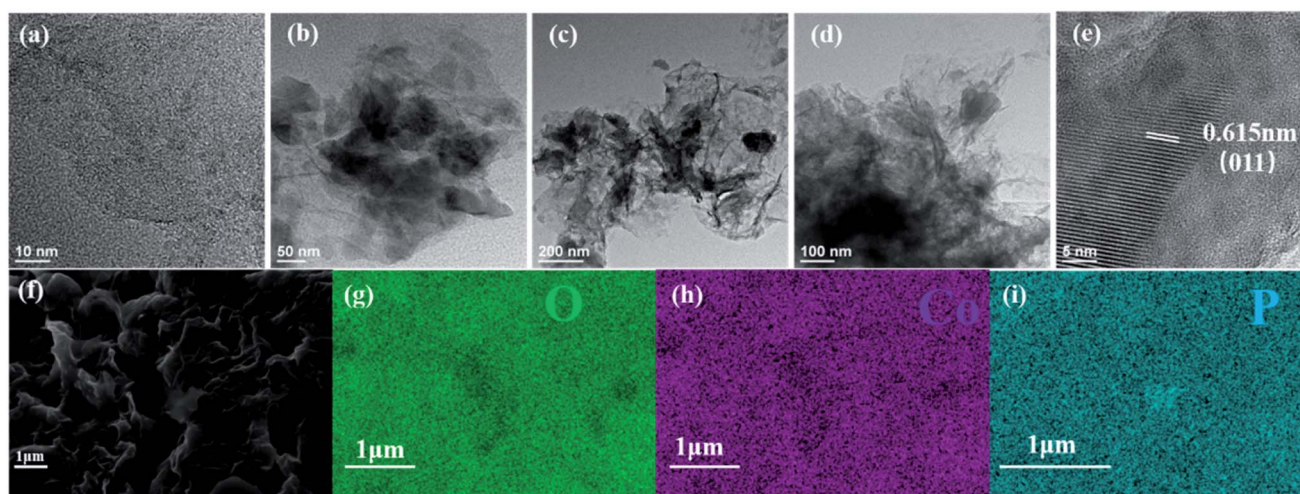

Fig. 2 (a) TEM images of 3D RGO, (b–e) TEM and HRTEM images of $Co(PO_3)_2$-3D RGO, (f–i) SEM images and Co, P, and O element mapping images of $Co(PO_3)_2$-3D RGO.

supporter for improving the conductivity of electrocatalysts and increasing their active area due to their unique physical and chemical properties. Different carbon materials will seriously affect the conductivity and active sites of electrocatalysts.[22,32,33]

Carbon materials include carbon black, carbon nanotubes, graphene and their derivatives.[12,15,36,37] Among the above materials, we choose three-dimensional graphene as the support of the catalyst, which has the advantages of large specific surface area, interconnected ordered pore structure, abundant active sites, excellent electrical conductivity, lightweight and good mechanical strength comparing with other carbon materials.[22,34,35] These advantages can enhance the electron transport capacity of the electrocatalyst, increase the contact area between the catalyst and the electrolyte solution, and accelerate the release of reaction gases.[32,38,39] Zheng et al.[40] synthesized RGO/CoP-Rh through the interaction between three-dimensional graphene and the material, which showed excellent hydrogen evolution ability but only in acidic electrolyte.

To sum up, in this work, we loaded the cobalt phosphate-based electrocatalyst on the three-dimensional graphene with good conductivity and stability. We synthesized the Zeolitic
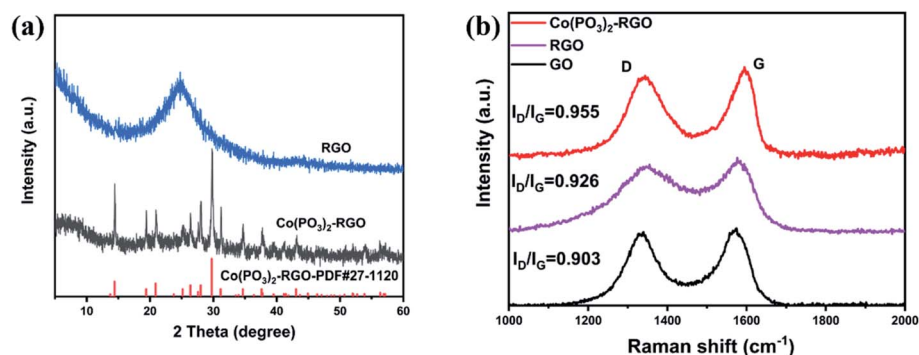

Fig. 3 (a) XRD patterns of 3D RGO, Co(PO₃)₂-3D RGO, (b) Raman patterns of 3D RGO, Co(PO₃)₂-3D RGO.
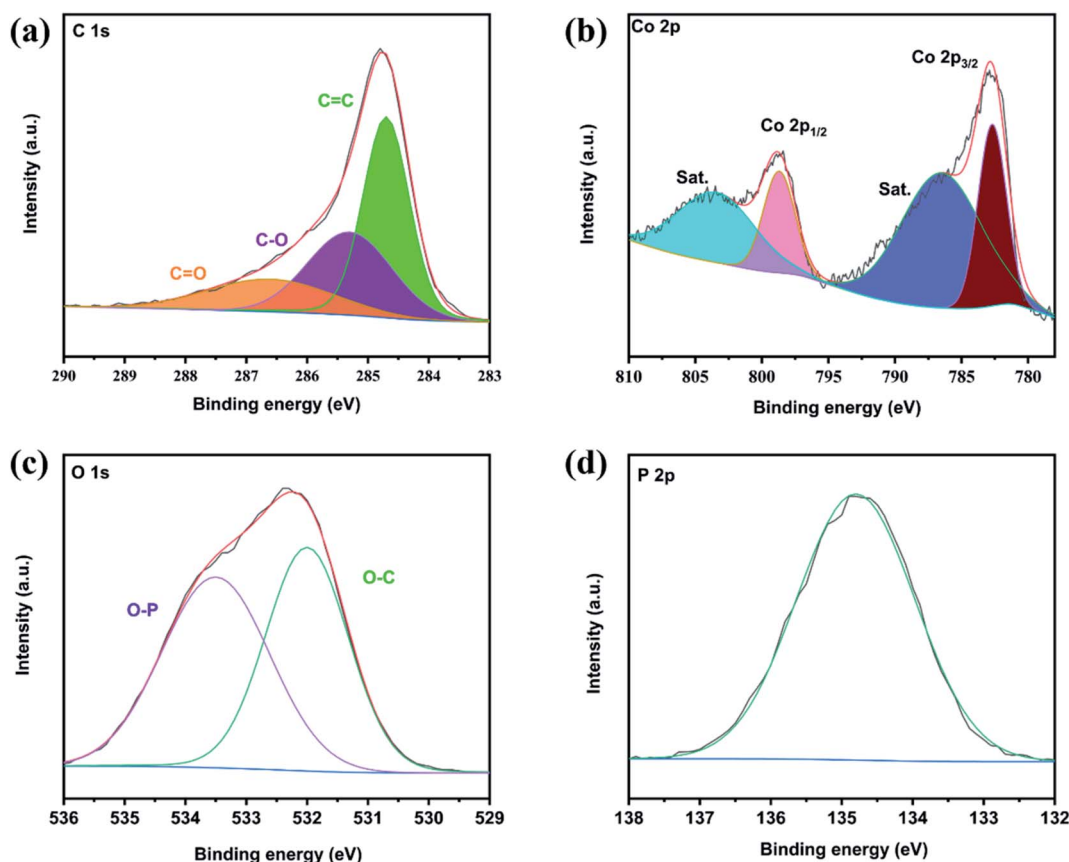

Fig. 4 High resolution XPS of (a) C 1s spectrum, (b) Co 2p spectrum, (c) O 1s spectrum, (d) P 2p spectrum.

Imidazolate Framework-67 (ZIF-67) precursor that owns more active sites through Co^{2+} and 2-methylimidazole, which was applied to prepare three-dimensional graphene-supported cobalt metaphosphate ($Co(PO_3)_2$-3D RGO) by PH_3 assisted at low temperature. A simple PH_3-assisted synthesis of three-dimensional reduced graphene oxide-supported metaphosphate was proposed. This work provides a new idea and method for loading HER electrocatalyst on three-dimensional graphene.

Results and discussion

Characterizations of Co(PO₃)₂-3D RGO

The structures of $Co(PO_3)_2$-3D RGO and RGO were observed with high-performance thermal field scanning electron microscope and field emission transmission electron microscope. The SEM image shows that the prepared graphene and the catalyst both present a three-dimensional porous hierarchical structure. Graphene oxide is a corrugated sheet structure, which is reduced by hydrothermal process to yield reduced graphene oxide. It can be seen from Fig. 1 that reduced graphene oxide is a three-dimensional porous hierarchical structure composed of many folded sheets, which has a rich pore structure that is beneficial for the conduction and transportation of electron.[41] It is an excellent carrier that is suitable perfectly for using as an electrocatalyst, which proves that the reduced graphene oxide is

successfully prepared after hydrothermal reduction. The high-magnification morphological image of $Co(PO_3)_2$-3D RGO can be seen clearly in Fig. 2. EDS mapping is performed on the surface of Fig. 2f. From the EDS element distribution diagram, it can be seen that the Co and P elements are uniformly loaded on the three-dimensional graphene substrate. After loading Co and P elements on graphene, the porous structure of graphene can still be clearly seen, in which electrolyte solution circulates. It can increase the contact area between the catalyst and the electrolyte solution and accelerate the release of gas in the pores. The porous electrocatalyst has great advantages in the HER. As shown in Fig. 2b–d, the TEM image shows that $Co(PO_3)_2$ is uniformly loaded on graphene. As shown in Fig. 2e, the high-resolution TEM (HRTEM) image exhibit that $Co(PO_3)_2$ has a 0.615 nm crystal plane spacing, which correspond to the (011) crystal plane of $Co(PO_3)_2$ (PDF#27-1120).

XRD and Raman tests further proved that $Co(PO_3)_2$-3D RGO was prepared successfully. As shown in Fig. 3a, the characteristic diffraction peaks of $Co(PO_3)_2$-3D RGO are at 14.4, 19.4, 20.9, 25.2, 26.4, 28.0, 29.7, 31.2, 34.7, 37.6 and 43.1° corresponding to (011), (−211), (−112), (211), (121), (310), (−222), (013), (400), (222), (−233) crystal planes of $Co(PO_3)_2$ respectively (PDF#27-1120). The diffraction peak of $Co(PO_3)_2$-3D RGO corresponds completely to the PDF standard card, which indicates that PH_3 assisted synthesis can completely convert ZIF67 into $Co(PO_3)_2$. In Fig. 3a, you can see the comparison of the XRD
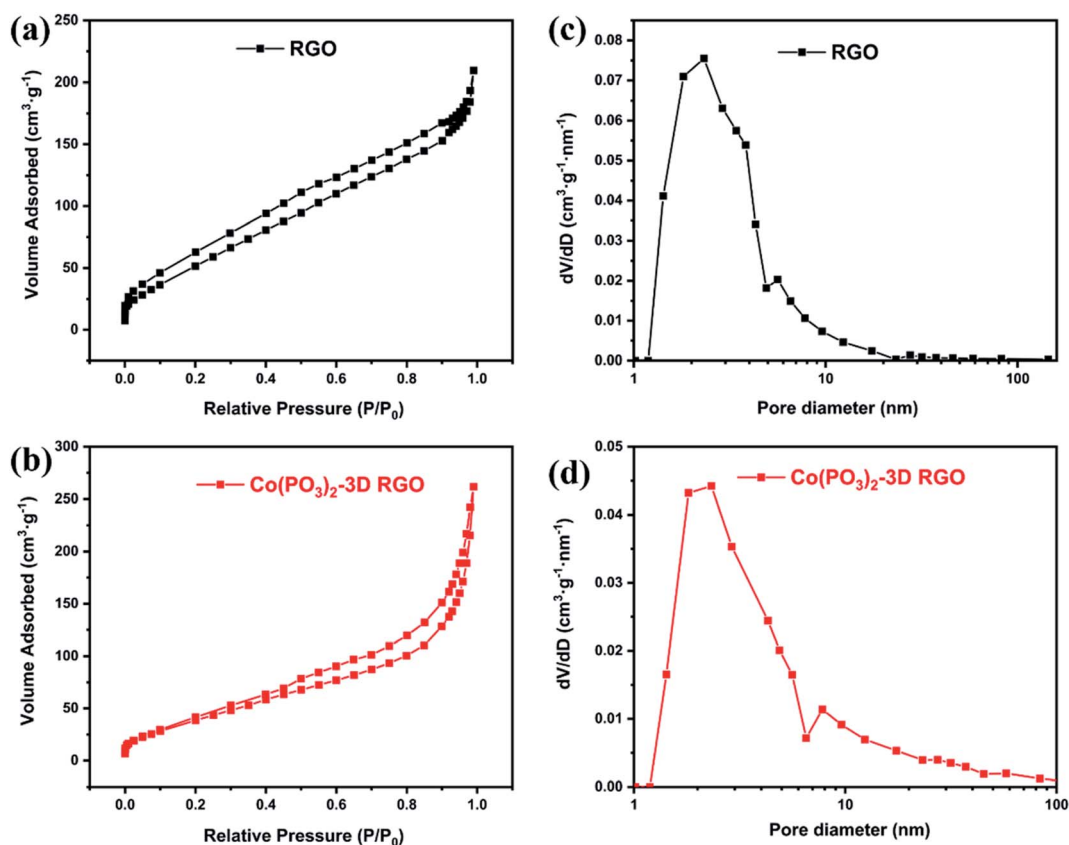

Fig. 5 N^2 adsorption−desorption isotherm of (a) 3D RGO, (b) $Co(PO_3)_2$-3D RGO, pore size distribution curve of (c) 3D RGO, (d) $Co(PO_3)_2$-3D RGO.

spectra of RGO and $Co(PO_3)_2$-3D RGO. From the RGO spectrum, we can see an obvious broad diffraction peak at 24.6°. $Co(PO_3)_2$-3D RGO has some diffraction peaks at 5° to 30°, so the diffraction characteristic peaks of RGO are not quite obvious. $Co(PO_3)_2$-3D RGO exhibited the best HER performance among the prepared materials with different ratios, so the following characterizations are all centered on it. The Raman spectra of GO and $Co(PO_3)_2$-3D RGO are shown in Fig. 3b. Two obvious strong peaks can be seen from the Raman spectrum, the peak positions are respectively at 1590 and 1340 cm^{-1}, corresponding to the G and D bands of GO. The obvious D peak and G peak indicate that there are many defects in the material. The ratio of I_D/I_G is related to the degree of defect of the material. The I_D/I_G ratio of $Co(PO_3)_2$-3D RGO is 0.955, higher than that of RGO(0.926) and GO(0.903), which can further indicate that the degree of defect of graphene increases with the loading of cobalt metaphosphate.

Then the composition and chemical state of $Co(PO_3)_2$-3D RGO were further studied by X-ray photoelectron spectroscopy (XPS). As shown in Fig. 4, the XPS test verifies the presence of C, Co, P and O elements. As shown in Fig. 4a, the high-resolution profile of C1s exhibits three peaks of C at 284.7, 285.3, and 286.6 eV, which can correspond to C=C, C–O, and C=O respectively.[4,8,12,42] The peaks of C=O and C–O are obviously weaker than the peaks of C=C. It may be that most of the

oxygen-containing groups of GO were removed during the hydrothermal process to form RGO. As shown in Fig. 4b, four peaks can be found in the pattern of Co 2p, at 782.7, 786.5, 798.7 and 803.4 eV. The peaks at 782.7 eV and 798.7 eV belong to Co 2p3/2 and Co 2p1/2 respectively. There are also two satellite peaks at 786.5 eV and 803.4 eV, which are characteristic peaks of Co^{2+} ions.[12,22,29,38] In Fig. 4c, the XPS peaks of O1s at 532 and 533.5 eV correspond to O–P bonds and O–C bonds, respectively.[38] As shown in Fig. 4d, the P peak at 344.8 eV corresponds exactly to the P–O bond of $(PO_3)^{2-}$,[22] which the O–P bond corresponding exactly to the peak of O1s 532 eV that belongs to the O–P bond. The results of XPS further proved that we successfully synthesized $Co(PO_3)_2$-3D RGO.

To further explore the properties of $Co(PO_3)_2$-3D RGO. We analyzed and tested the specific surface area and pore size distribution of RGO and $Co(PO_3)_2$-3D RGO, of which the nitrogen adsorption and desorption isotherms and pore size distribution diagrams are shown in the Fig. 5. The BET curve of RGO and $Co(PO_3)_2$-3D RGO are shown in Fig. 5a and b. The adsorption curve of the material is similar to type IV. The specific surface area of $Co(PO_3)_2$-3D RGO that is calculated by BET (Brunauer–Emmert–Teller) method is 257.2 $m^2\ g^{-1}$ smaller than 360.1 $m^2\ g^{-1}$ of RGO, which indicates that $Co(PO_3)_2$ being loaded on graphene decreases the specific surface area of the material. This is because the pores are blocked after calcination.

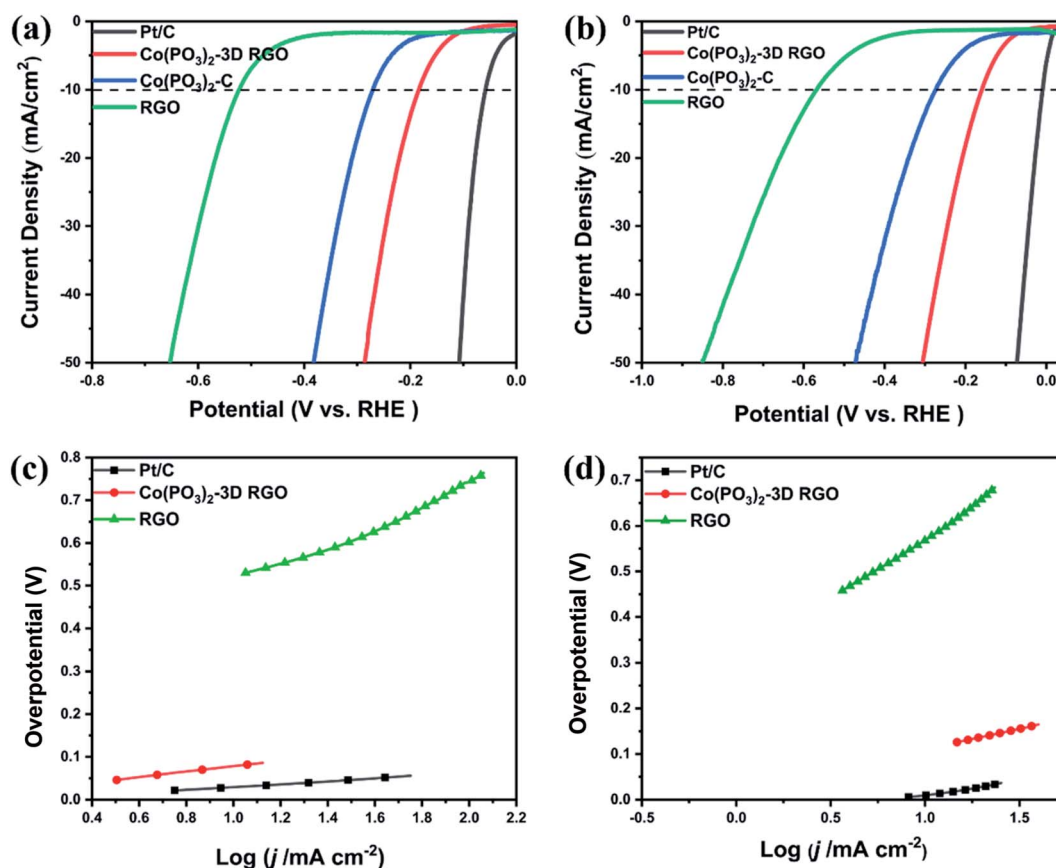**Fig. 6** LSV curves of Pt/C, $Co(PO_3)_2$-3D RGO, $Co(PO_3)_2$-C and RGO at a scan rate of 5 mV s^{-1} (a) in 0.5 M H_2SO_4, (b) in 1 M KOH, Tafel plots of Pt/C, $Co(PO_3)_2$-3D RGO and RGO (c) in 0.5 M H_2SO_4, (d) in 1 M KOH.

Table 1 Hydrogen evolution performance of different types of cobalt-based and three-dimensional graphene-based electrocatalysts

| Electrocatalyst | HER performances in 0.5 M H_2SO_4 | | HER performances in 1 M KOH | | References |
	η_{10} (mV)	Tafel slope (mV dec^{-1})	η_{10} (mV)	Tafel slope (mV dec^{-1})	
Co–Co$_2$P@CNT/rGO	210	55.43	—	—	5
MoS$_2$-PRGO	186	35	—	—	12
CoP/Co$_2$P-RGO	156	53.8	—	—	13
CoMnP@NG	164	65	140	111	17
CoP@NC-NG	135	59.3	155	68.6	20
CoP-NRGO	—	—	184	190	25
CoP@NRGO	90	87	—	—	26
CoP/RGO-PL	168	57	—	—	28
CoP-GA	121	50	—	—	33

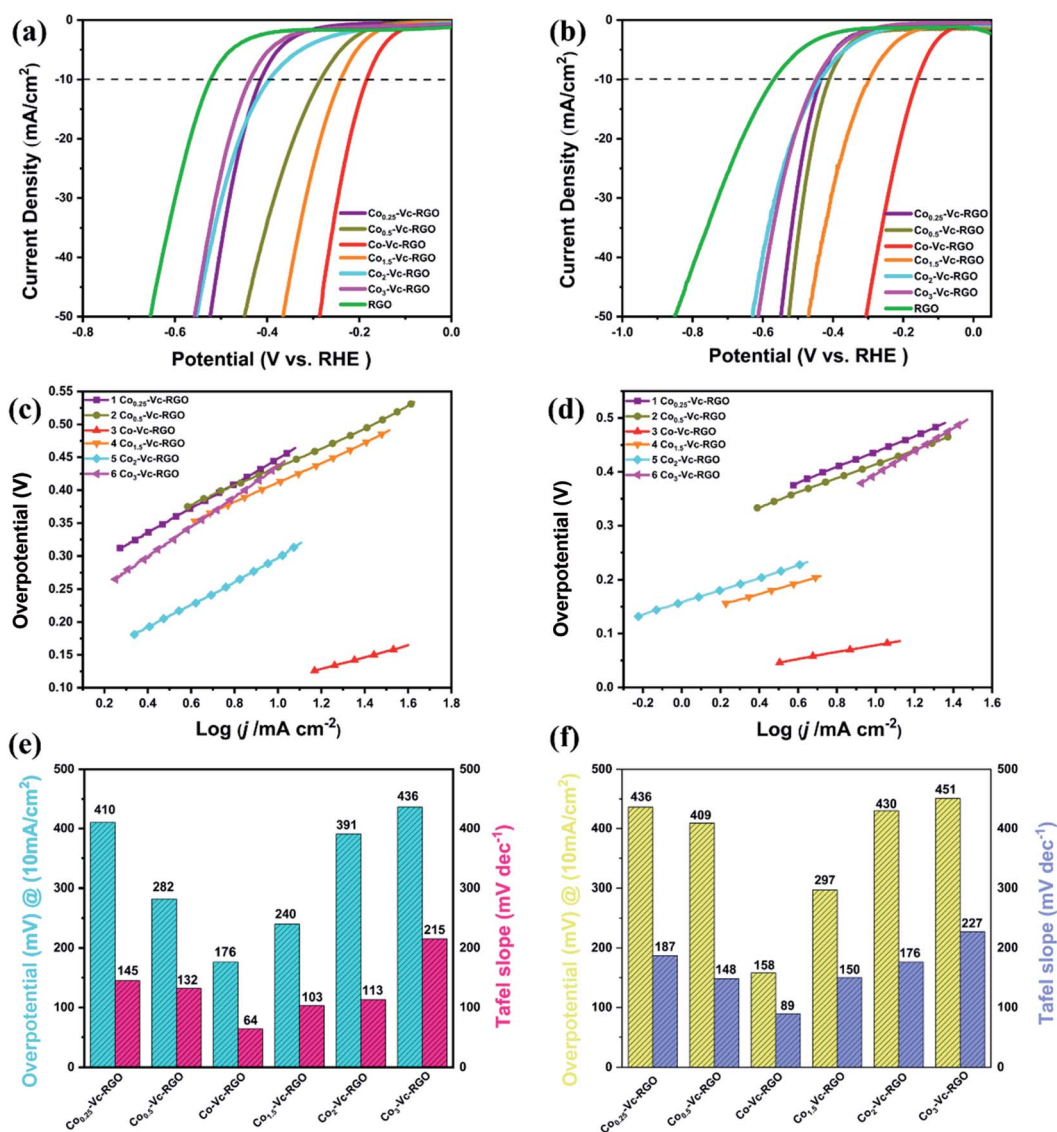**Fig. 7** LSV curves for Co$_{0.25}$-Vc-RGO, Co$_{0.5}$-Vc-RGO, Co-Vc-RGO, Co$_{1.5}$-Vc-RGO, Co$_2$-Vc-RGO and Co$_2$-Vc-RGO (labeled 1–6) at a scan rate of 5 mV s^{-1}, (a) in 0.5 M H_2SO_4, (b) in 1 M KOH. Tafel plots of samples 1–6 (c) in 0.5 M H_2SO_4, (d) in 1 M KOH, overpotential (the current density at 10 mA cm^{-2}) and Tafel plots of samples 1–6 (e) in 0.5 M H_2SO_4, (f) in 1 M KOH.

The pore size distribution diagrams of RGO and $Co(PO_3)_2$-3D RGO are shown in Fig. 5c and d. The pore size distribution is calculated by the BJH (Barrett–Joyner–Halenda) method. The pore size of $Co(PO_3)_2$-3D RGO is mainly distributed between 1–10 nm, which belongs to micropores. Compared with RGO, the number and pore diameter of $Co(PO_3)_2$-3D RGO are slight increase. Due to the measurement aperture range of 0–100 nm, 3D graphene has many pore structures larger than 100 nm which are not shown in the figure. But it can be clearly seen in Fig. 1d and e.

Electrochemical performance of the as-made samples

The LSV curves of 20% commercial Pt/C, RGO and $Co(PO_3)_2$-3D RGO as working electrodes are shown in Fig. 6. In 0.5 M H_2SO_4 solution, the Pt/C catalyst undoubtedly shows the best HER performance, which only needs 56 mV to obtain a current density of 10 mA cm^{-2}. The LSV curves of $Co(PO_3)_2$-3D RGO, $Co(PO_3)_2$-C and RGO are shown in Fig. 6a. They require 176, 269 and 520 mV to reach 10 mA cm^{-2}, respectively. In 1 M KOH solution, the Pt/C catalyst also showed the most excellent HER performance among the above four materials, which only needs 11 mV to obtain a current density of 10 mA cm^{-2}. The LSV curves of $Co(PO_3)_2$-3D RGO, $Co(PO_3)_2$-C and RGO are shown in Fig. 6b. They require 158, 270 and 571 mV to reach 10 mA cm^{-2},

respectively. The Tafel plots of Pt/C, $Co(PO_3)_2$-3D RGO and RGO are shown in Fig. 5c and d. Although Pt/C catalyst has excellent HER performance, the excessive cost and scarcity of Pt severely hinder its wide application in the field of electrocatalytic water splitting. Cobalt metaphosphate-based materials exactly have the advantages of being cheap, clean and simple to prepare.[24–27] It can be clearly seen from Fig. 6, the HER performance of $Co(PO_3)_2$-3D RGO is better than that of $Co(PO_3)_2$-C, which shows that it is a correct choice for us to load cobalt metaphosphate on three-dimensional graphene. It can enhance the hydrogen evolution ability of $Co(PO_3)_2$ material in acid or alkali. This is closely related to the increase in the specific surface area and pore size of the material. As the specific surface area and the pore size increases, the electron transport capacity of the catalyst is enhanced, and the contact area with the electrolyte will also increase, which can also accelerate the release of gas and the circulation of electrolyte solution.

As shown in Table 1, we compared the overpotentials and Tafel slopes of cobalt-based hydrogen evolution catalysts and graphene-supported hydrogen evolution catalysts in different electrolyte solutions, most of which can only perform in a single electrolyte solution. And a small number of catalysts can show good hydrogen evolution performance in both acidic and basic electrolyte solutions, but their preparation methods are slightly complicated. Therefore, we choose $Co(PO_3)_2$-3D RGO as the

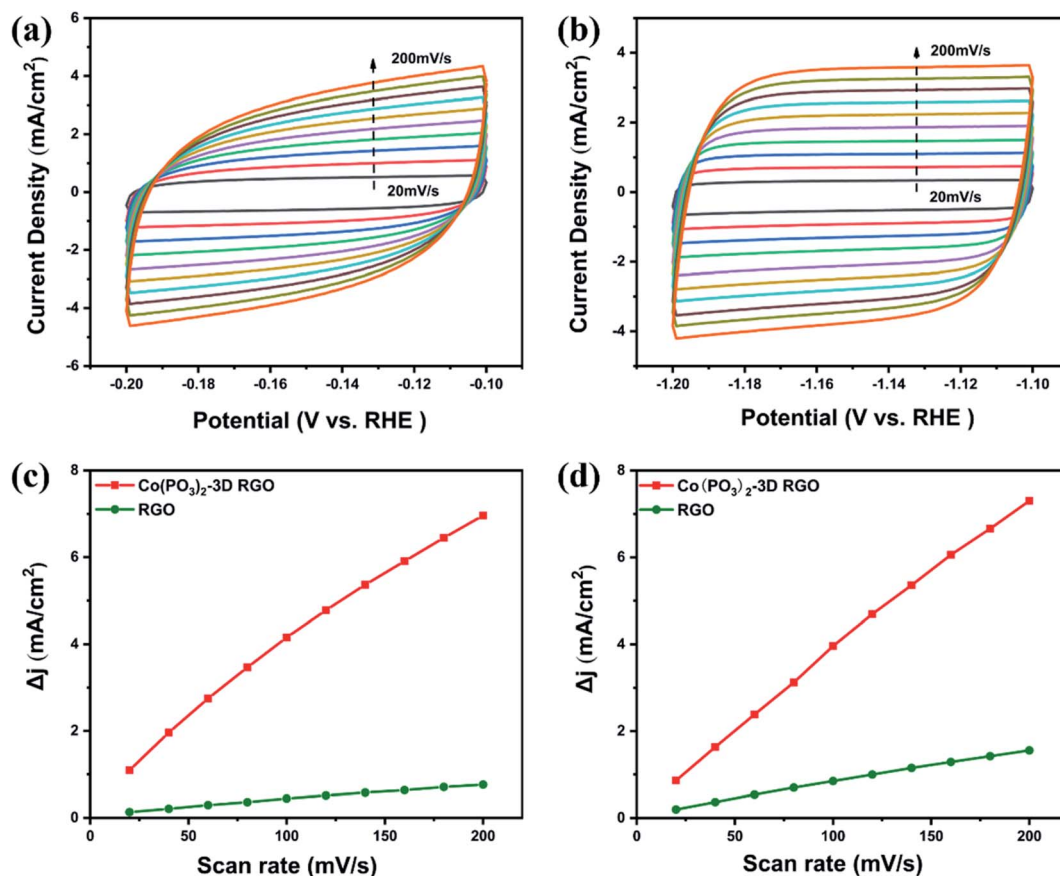Fig. 8 Cyclic voltammograms of $Co(PO_3)_2$-3D RGO at a scan rate of 20–200 mV s^{-1} (a) in 0.5 M H_2SO_4, (b) in 1 M KOH, ECSA plot of $Co(PO_3)_2$-3D RGO and RGO (c) in 0.5 M H_2SO_4, (d) in 1 M KOH.

studied material, which has a simple preparation method and exhibits good effects in two electrolyte solutions at the same time.

The LSV curves of the catalyst prepared by adding different proportions of Co and Vc using for reducing agent are shown in Fig. 7. The LSV curves of $Co_{0.25}$-Vc-RGO, $Co_{0.5}$-Vc-RGO, Co-Vc-RGO, $Co_{1.5}$-Vc-RGO, Co_2-Vc-RGO, Co_3-Vc-RGO in 0.5 M H_2SO_4 are shown in Fig. 7c, of which the required potentials that the current density reaches 10 mA cm^{-2} are 410, 282, 176, 240, 391, and 436 mV, respectively. The LSV curves of them in 1 M KOH are shown in Fig. 7, of which the required potentials that the current density reaches 10 mA cm^{-2} are 436, 409, 158, 297, 430 and 451 mV, respectively. As the amount of Co added increases,

the potential required when the current density reaches 10 mA cm^{-2} gradually decreases and then continues to increase. These results perfectly prove that the HER performance of the material is the best when the ratio of Co^{2+} and Vc is 1 : 1. In order to further prove that we use the formula $\eta = b \log j + a$ (b is the Tafel slope, j is the current density) to calculate the Tafel slope of the obtained LSV curve. It can be clearly seen from Fig. 8c that when the ratio of Co^{2+} and Vc is 1 : 1, the minimum Tafel slope is 64 mV dec^{-1} in 0.5 M H_2SO_4. The Tafel slopes of other samples are shown in Fig. 7c respectively. As shown in Fig. 7d, when the ratio of Co^{2+} and Vc is 1 : 1, the minimum Tafel slope is 88 mV dec^{-1} in 1 M KOH. The Tafel slopes of other samples are shown in Fig. 7d respectively. From the histograms in Fig. 7e

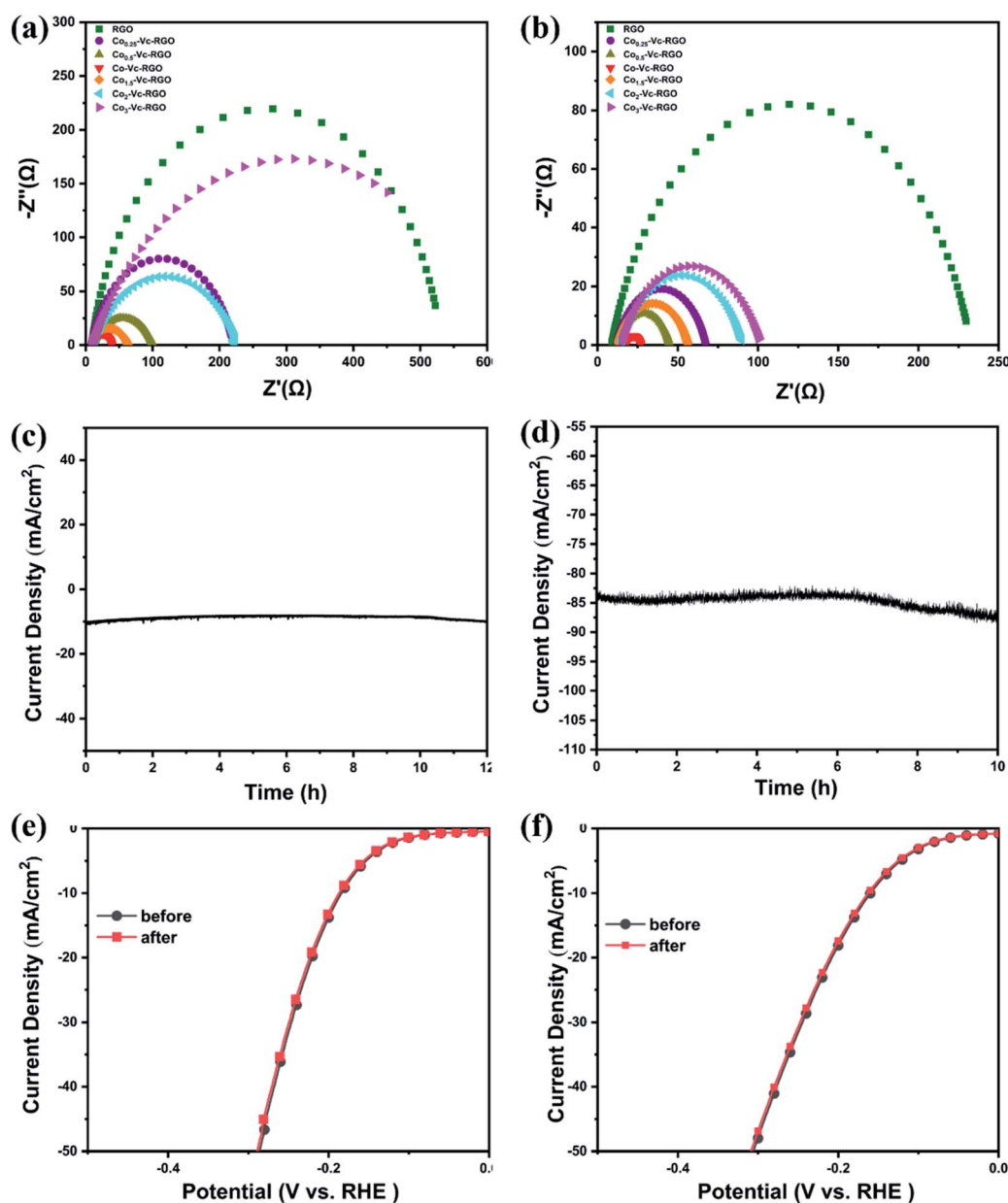Fig. 9   EIS Nyquist plots of samples 1–6 (a) at −0.6 V (vs. Ag/AgCl) in 0.5 M H_2SO_4, (b) at −1.6 V (vs. Ag/AgCl) in 1 M KOH, Time-dependent current density curve for $Co(PO_3)_2$-3D RGO (c) at an overpotential of 176 mV in 0.5 M H_2SO_4, (d) at an overpotential of 393 mV in 1 M KOH, The polarization curve of $Co(PO_3)_2$-3D RGO before and after 1000 cycles of a durability test (e) in 0.5 M H_2SO_4, (f) in 1 M KOH.

and f, we can clearly see the potential required for the samples of different proportions to reach the current density of 10 mA cm^{-2} and the Tafel slope obtained from the LSV curve. In summary, it is shown that the optimal ratio of Co^{2+} and Vc is 1 : 1, which also further illustrates the fast electrochemical hydrogen evolution rate and rapid reaction kinetics of $Co(PO_3)_2$-3D RGO.

In order to further prove the rapid reaction kinetics of $Co(PO_3)_2$-3D RGO, we performed cyclic voltammetry tests on the carrier 3D RGO and the material $Co(PO_3)_2$-3D RGO, in which the scanning speed was 20–200 mV s^{-1}. As shown in Fig. 8a and b, the CV curve of the material $Co(PO_3)_2$-3D RGO is symmetrical in both acid and alkali, which indicates that the material is very stable.[43,44] As shown in Fig. 8c and d, then the electrochemical active surface area (ECSA) of the material is calculated based on the double-layer capacitance. In 1 M KOH solution, the ECSA of RGO and material $Co(PO_3)_2$-3D RGO are 8.1 and 37.7 mF cm^{-2}, respectively; in 0.5 M H_2SO_4 solution, the ECSA of RGO and material $Co(PO_3)_2$-3D RGO are 4.1 and 37.5 mF cm^{-2}, respectively. The ECSA of the material is much higher than that of the carrier RGO, which indicates that the active sites increase after loading the material. And it also shows that $Co(PO_3)_2$-3D RGO has fast reaction kinetics. The CV curve of the material is symmetric well, which shows that the material possesses excellent stability.[43,44] Therefore, we have further tested the stability of the material.

As shown in Fig. 9c–f, we judge the stability of the material by exploring the relationship between the current density of the material and the time under constant potential. The time-dependent current density curve at a static overpotential of 176 and 158 mV indicated that $Co(PO_3)_2$-3D RGO maintained its catalytic activity for at least 10 h (Fig. 5c and d). Next, we performed electrochemical impedance spectroscopy (EIS) tests on the prepared samples as shown in Fig. 9a and b. According to the equivalent circuit, the Nyquist diagrams of all materials present a regular semicircle. Among them, the resistance of the carrier RGO is the largest, and the resistance of the material $Co(PO_3)_2$-3D RGO is the smallest, which indicates that the conductivity of the material is enhanced after loading cobalt metaphosphate on RGO. In summary, $Co(PO_3)_2$-3D RGO has excellent stability and outstanding kinetics, which indicates that it is suitable well for HER.

Conclusions

In this work, we prepared a cheap and efficient electrocatalyst cobalt-based metaphosphate using a low-temperature PH_3 assisted synthesis method. According to the analysis of the test results, the material $Co(PO_3)_2$-3D RGO that is prepared for the first time only needs 176 and 158 mV current density to reach 10 mA cm^{-2}, with the Tafel slope only 63 and 88 mV dec^{-1} in acid or alkaline solution. The material has excellent stability in both acidic and alkaline solutions, which possesses a small resistance that is shown in Impedance spectroscopy. And it owns a large specific surface area shown in the nitrogen adsorption and desorption isotherms. These advantages are all beneficial to improve the hydrogen evolution capacity of the

electrocatalyst. Loading metaphosphate on 3D graphene can not only improve the hydrogen evolution capacity of the material, but also increase the specific surface area and stability of the material, which provides a new idea for the synthesis of bifunctional electrocatalysts.

Experimental

Materials

Flake graphite powder (C), phosphorus pentoxide (P_2O_5, AR), potassium peroxydisulfate ($K_2S_2O_8$, AR), concentrated sulfuric acid (H_2SO_4, AR), potassium permanganate (KMnO$_4$, AR), hydrogen peroxide (H_2O_2, AR), Cobalt(II) nitrate hexahydrate ($Co(NO_3)_2 \cdot 6H_2O$, AR), 2-methylimidazole (2-MIM, $C_4H_6N_2$, 98%), ascorbic acid(Vc, $C_6H_8O_6$, AR), sodium hypophosphate monohydrate ($NaH_2PO_2 \cdot H_2O$, AR) bought from Sinopharm Chemical Reagent Co., Ltd (Shanghai, China).

Characterization

X-ray diffraction (XRD) patterns within the 2θ range of 5–80° were collected on a SmartlabSE 3 kW X-ray diffractometer (Cu Kα radiation) under a continuous scanning mode with the scanning rate of 10° min^{-1} and the step size of 0.02°. The morphologies and detailed structure were obtained from Zeiss GeminiSEM450 high performance thermal field scanning electron microscopy (SEM) and Tecnai G2 F30 transmission electron microscopy (TEM). Raman spectra were measured by a inVia Reflex using a 532 nm laser light source.

Synthesis of ZIF-67

Graphene oxide was synthesized by the improved hummers method with flake graphite powder. In a beaker with 0.1 mmol of cobalt nitrate hexahydrate, 30 mL of deionized water and 30 mL (1 mg mL^{-1}) of GO solution were added. The solution was ultrasonicated for 30 minutes to a uniform dispersion. After stirring for 30 minutes, add a small amount of 2-methylimidazole and deionized water to the beaker, and stir vigorously for two hours. A small amount of Vc was added and stirring was continued for two hours. The solution in the beaker was transferred to a Teflon-lined stainless steel autoclave, heated to 85 °C for 15 minutes in an oven, and then heated to 120 °C for 4 hours. Finally, after the solution is cooled to room temperature, which is rinsed with water and ethanol then suction filtered, and the sample is freeze-dried for 24 h. Keeping the other, conditions unchanged, the ratio of $Co(NO_3)_2 \cdot 6H_2O$ and Vc was changed to synthesize $Co_{0.25}$-Vc-RGO, $Co_{0.5}$-Vc-RGO, Co-Vc-RGO, $Co_{1.5}$-Vc-RGO, Co_2-Vc-RGO, Co_2-Vc-RGO respectively.

Synthesis of $Co(PO_3)_2$-3D RGO

$Co(PO_3)_2$-3D RGO is prepared by simple low-temperature phosphating with ZIF67 as the precursor. To prepare $Co(PO_3)_2$-3D RGO, 50 mg of ZIF-67 and 500 mg of NaH_2PO_2 are placed in one quartz boat, the P source is placed at one end of the porcelain circle near the air inlet of the tube furnace, and the sample is placed on the other end. The calcination

temperature was 350 °C, calcined for two hours, and the gas flow was 30 mL min^{-1} under nitrogen atmosphere.

Synthesis of Co(PO$_3$)$_2$-C

First, cobalt metaphosphate was synthesized. The preparation of cobalt metaphosphate was the same as that of Co(PO$_3$)$_2$-3D RGO without adding GO solution. Take 4 mg of Co(PO$_3$)$_2$ and 0.25 mg of conductive carbon powder in a vial, then add 500 μL ethanol, 500 μL water and 30 μL naphthol to the vial. Ultrasonic dispersion of the solution in the vial is the dispersion of Co(PO$_3$)$_2$-C.

Preparation of the working electrode and electrochemical measurements

The electrochemical test of all samples includes linear sweep voltammetry (LSV), cyclic voltammetry (CV), current–time curve (it curve) test, electrochemical impedance spectroscopy (EIS), which were measured by using a standard three-electrode system and electrochemical workstation CHI660D (Shanghai Chenhua, China). All tests were performed with IR compensation and the compensation result was 100%. Saturated silver/silver chloride electrode, graphite rod electrode, glassy carbon electrode are used as reference electrode, counter electrode and working electrode, respectively. All tests are carried out in H$_2$SO$_4$ (0.5 mol L^{-1}) and KOH (1 mol L^{-1}) solutions at room temperature. The electrocatalytic activity for HER was evaluated by measuring polarization curves using LSV with the scan rate of 5 mV s^{-1}. In the frequency range of 100 kHz to 0.1 Hz, the EIS test was performed at a constant potential of −0.6 V (vs. RHE) in 0.5 M H$_2$SO$_4$, and a constant potential of −1.6 V (vs. RHE) in 1 M KOH. The Tafel slope is calculated from the LSV curve at different ratios. The cyclic voltammetry test is measured under the condition of a scanning speed of 20–200 mV. Preparation of working electrode: Take 4 mg of sample and add it to a vial containing 500 μL ethanol, 500 μL distilled water, and 30 μL Nafion solution. The sample solution was ultrasonicated to a uniform dispersion, and 5 μL of the solution was dropped on a 3 mm diameter glassy carbon electrode (the catalyst loading on the glassy carbon electrode was 0.283 mg cm^{-2}), which was dried naturally under a warm lamp.

Author contributions

Zijie Tang: Conceptualization, Methodology, Software, Investigation, Writing-original draft, preparation, Writing – Review & Editing. Shenqi Wei: Methodology, Investigation, Visualization. Yuanyuan Wang: Resources, Supervision, Visualization, Funding acquisition, Writing – Review & Editing. Liyi Dai: Resources, Supervision, Visualization, Writing – Review & Editing.

Conflicts of interest

There are no conflicts to declare.

Acknowledgements

Notes and references

1 X. Kong, P. Gao, R. Jiang, J. Feng, P. Yang, S. Gai, Y. Chen, Q. Chi, F. Xu and W. Ye, Orderly layer-by-layered TiO$_2$/carbon superstructures based on MXene's defect engineering for efficient hydrogen evolution, *Appl. Catal., A*, 2020, **590**, 117341.

2 X. Ren, F. Xu, Z. Peng, Q. Chi, W. Li, J. Wang, T. Tao, W. Ye and P. Gao, Boosting visible light driven hydrogen production: Bifunctional interface of Ni(OH)$_2$/Pt cocatalyst on TiO$_2$, *Int. J. Hydrogen Energy*, 2020, **45**, 16614–16621.

3 H. Shen, D. Ni, P. Niu, Y. Zhou, T. Zhai and Y. Ma, Enhancing photocatalytic H$_2$ evolution from water on CuO-Co$_3$O$_4$/TiO$_2$: The key roles of Co$_3$O$_4$ loading amounts, *Int. J. Hydrogen Energy*, 2017, **42**, 30559–30568.

4 A. Adam, M. H. Suliman, H. Dafalla, A. R. Al-Arfaj, M. N. Siddiqui and M. Qamar, Rationally dispersed molybdenum phosphide on carbon nanotubes for the hydrogen evolution reaction, *ACS Sustainable Chem. Eng.*, 2018, **6**, 11414–11423.

5 L. Chen, P. Wu, C. Zhu, S. Yang, K. Qian, N. Ullah, W. Wei, C. Sun, Y. Xu and J. Xie, Fabrication of carbon nanotubes encapsulated cobalt phosphide on graphene: cobalt promoted hydrogen evolution reaction performance, *Electrochim. Acta*, 2020, **330**, 135213.

6 R. Dong, A. Zhu, W. Zeng, L. Qiao, L. Lu, Y. Liu, P. Tan and J. Pan, Selective phosphidation and reduction strategy to construct heterostructured porous nanorod of CoP coated on Mn$_3$O$_4$ as a bifunctional electrocatalyst for overall water splitting, *Appl. Surf. Sci.*, 2021, **544**, 148860.

7 Y. Wang, H. Li, Q. Yao, R. Li, Z. Guo, H. Chen, K. Qu and R. Li, Highly dispersed cobalt metaphosphate nanoparticles embedded in tri-doped carbon as a pH-wide electrocatalyst for hydrogen evolution, *Int. J. Hydrogen Energy*, 2021, **46**, 6513–6521.

8 H. Huang, C. Yu, J. Yang, X. Han, C. Zhao, S. Li, Z. Liu and J. Qiu, Ultrasmall diiron phosphide nanodots anchored on graphene sheets with enhanced electrocatalytic activity for hydrogen production via high-efficiency water splitting, *J. Mater. Chem. A.*, 2016, **4**, 16028–16035.

9 J. Huang, M. Chen, X. Zhang, W. Liu and Y. Liu, P-doped 3D graphene network supporting uniformly vertical MoS$_2$ nanosheets for enhanced hydrogen evolution reaction, *Int. J. Hydrogen Energy*, 2020, **45**, 4043–4053.

10 T. S. Kim, H. J. Song, M. A. Dar, H. W. Shim and D. W. Kim, Thermally reduced rGO-wrapped CoP/Co$_2$P hybrid microflower as an electrocatalyst for hydrogen evolution reaction, *J. Am. Ceram. Soc.*, 2018, **101**, 3749–3754.

11 J.-S. Li, J.-Y. Li, M.-J. Huang, L.-X. Kong and Z. Wu, Anchoring Ru$_x$P on 3D hollow graphene nanospheres as efficient and pH-universal electrocatalysts for the hydrogen evolution reaction, *Carbon*, 2020, **161**, 44–50.

12 L. Li, X. Wang, Y. Guo and J. Li, Synthesis of an ultrafine CoP nanocrystal/graphene sandwiched structure for

efficient overall water splitting, *Langmuir*, 2020, **36**, 1916–1922.

13 J. Liu, W. Li, Z. Cui, J. Li, F. Yang, L. Huang, C. Ma and M. Zeng, CoMn phosphide encapsulated in nitrogen-doped graphene for electrocatalytic hydrogen evolution over a broad pH range, *Chem. Commun.*, 2021, **57**, 2400–2403.

14 Y. Sun, K. Xu, Z. Zhao, X. Li, G. Chen and C. Li, Strongly coupled dual zerovalent nonmetal doped nickel phosphide nanoparticles/N, B-graphene hybrid for pH-universal hydrogen evolution catalysis, *Appl. Catal., B*, 2020, **278**, 119284.

15 K. Kohila Rani, C. Karuppiah, S. F. Wang, S. O. Alaswad, P. Sireesha, R. Devasenathipathy, R. Jose and C. C. Yang, Direct pyrolysis and ultrasound assisted preparation of N, S co-doped graphene/Fe₃C nanocomposite as an efficient electrocatalyst for oxygen reduction and oxygen evolution reactions, *Ultrason. Sonochem.*, 2020, **66**, 105111.

16 H. Chen, Z. Yang, J. Wu, Y. Rong and L. Deng, Industrial VN@reduced graphene oxide cathode for aqueous zinc ion batteries with high rate capability and long cycle stability, *J. Power Sources*, 2021, **507**, 230286.

17 F. Zeng, T. Lu, W. He, S. Chu, Y. Qu and Y. Pan, In-situ carbon encapsulation of ultrafine VN in yolk-shell nanospheres for highly reversible sodium storage, *Carbon*, 2021, **175**, 289–298.

18 W. Li, D. Liu, N. Yang, J. Wang, M. Huang, L. Liu, X. Peng, G. Wang, X.-F. Yu and P. K. Chu, Molybdenum diselenide–black phosphorus heterostructures for electrocatalytic hydrogen evolution, *Appl. Surf. Sci.*, 2019, **467**, 328–334.

19 Z. Chen, Q. Kang, G. Cao, N. Xu, H. Dai and P. Wang, Study of cobalt boride-derived electrocatalysts for overall water splitting, *Int. J. Hydrogen Energy*, 2018, **43**, 6076–6087.

20 X. Zhang, Y. Han, L. Huang and S. Dong, 3D Graphene Aerogels Decorated with Cobalt Phosphide Nanoparticles as Electrocatalysts for the Hydrogen Evolution Reaction, *ChemSusChem*, 2016, **9**, 3049–3053.

21 M. Wang, R. Ding, X. Cui, L. Qin, J. Wang, G. Wu, L. Wang and B. Lv, CoP porous hexagonal nanoplates in situ grown on RGO as active and durable electrocatalyst for hydrogen evolution, *Electrochim. Acta*, 2018, **284**, 534–541.

22 H. Wang, Q. Gao, S. Sun, W. Zhang and S. Yao, CoP@NRGO composite as a high-efficiency water electrolysis catalyst for hydrogen generation, *J. Solid State Chem.*, 2020, **290**, 121596.

23 T. Veettil Vineesh, U. Vijayakumar Anagha, N. Purayil Dileep, H. Cheraparambil, J. Nambeesan and M. M. Shaijumon, Enhanced bifunctional catalytic activity of cobalt phosphide flowers anchored N-doped reduced graphene oxide for hydrogen and oxygen evolution, *ChemElectroChem*, 2020, **7**, 3319–3323.

24 H. A. Höppe and J. M. U. Panzer, Crystal structure, vibrational spectra and activation of BaCa(P₄O₁₂) with Eu²⁺ Compared with β-Sr(PO₃)₂: Eu, *Eur. J. Inorg. Chem.*, 2009, **2009**, 3127–3130.

25 Y. Li, Z. Wang, J. Hu, S. Li, Y. Du, X. Han and P. Xu, Metal–organic frameworks derived Interconnected bimetallic metaphosphate nanoarrays for efficient electrocatalytic oxygen evolution, *Adv. Funct. Mater.*, 2020, **30**, 1910498.

26 X. Li, X. Xiao, Q. Li, J. Wei, H. Xue and H. Pang, Metal (M = Co, Ni) phosphate based materials for high-performance supercapacitors, *Inorg. Chem. Front.*, 2018, **5**, 11–28.

27 H. Zhao and Z. Yuan, Insights into transition metal phosphate materials for efficient electrocatalysis, *ChemCatChem*, 2020, **12**, 3797–3810.

28 H. S. Ahn and T. D. Tilley, Electrocatalytic water oxidation at neutral pH by a nanostructured Co(PO₃)₂ anode, *Adv. Funct. Mater.*, 2013, **23**, 227–233.

29 R. Gond, D. K. Singh, M. Eswaramoorthy and P. Barpanda, Sodium cobalt metaphosphate as an efficient oxygen evolution reaction catalyst in alkaline solution, *Angew. Chem., Int. Ed.*, 2019, **58**, 8330–8335.

30 C.-Z. Yuan, Y.-F. Jiang, Z. Wang, X. Xie, Z.-K. Yang, A. B. Yousaf and A.-W. Xu, Cobalt phosphate nanoparticles decorated with nitrogen-doped carbon layers as highly active and stable electrocatalysts for the oxygen evolution reaction, *J. Mater. Chem. A*, 2016, **4**, 8155–8160.

31 L.-H. Xu, S.-L. Zhang, S.-Y. Guo, X.-J. Zhang, S. Cosnier, R. S. Marks, W.-J. Wang, H.-B. Zeng and D. Shan, ATMP derived cobalt-metaphosphate complex as highly active catalyst for oxygen reduction reaction, *J. Catal.*, 2020, **387**, 129–137.

32 Y. Lu, Y. Ma, T. Zhang, Y. Yang, L. Wei and Y. Chen, Monolithic 3D cross-linked polymeric graphene materials and the likes: preparation and their redox catalytic applications, *J. Am. Chem. Soc.*, 2018, **140**, 11538–11550.

33 X. H. Xia, D. L. Chao, Y. Q. Zhang, Z. X. Shen and H. J. Fan, Three-dimensional graphene and their integrated electrodes, *Nano Today*, 2014, **9**, 785–807.

34 S. Dursun, R. G. Akay and M. S. Yazici, CVD graphene supported cobalt (II) phthalocyanine as cathode electrocatalyst for PEM fuel cells, *Int. J. Hydrogen Energy*, 2020, **45**, 34837–34844.

35 S. K. S. Hossain, M. M. Alwi, J. Saleem, H. T. Al-Hashem, G. McKay, S. Mansour and S. S. Ali, Bimetallic Pd-Co nanoparticles supported on nitrogen-doped reduced graphene oxide as efficient electrocatalysts for formic acid electrooxidation, *Catalysts*, 2021, **11**, 910.

36 C. Huang, C. Li and G. Shi, Graphene based catalysts, *Energy Environ. Sci.*, 2012, **5**, 8848–8868.

37 X. Lv and S. Yin, CoP-embedded nitrogen and phosphorus co-doped mesoporous carbon nanotube for efficient hydrogen evolution, *Appl. Surf. Sci.*, 2021, **537**, 147834.

38 J. Ma, M. Wang, G. Lei, G. Zhang, F. Zhang, W. Peng, X. Fan and Y. Li, Polyaniline derived N-doped carbon-coated cobalt phosphide nanoparticles deposited on N-doped graphene as an efficient electrocatalyst for hydrogen evolution reaction, *Small*, 2018, **14**, 1702895.

39 L. Wang and M. Pumera, Electrochemical catalysis at low dimensional carbons: graphene, carbon nanotubes and beyond–a review, *Appl. Mater. Today*, 2016, **5**, 134–141.

40 H. Zheng, X. Huang, H. Gao, W. Dong, G. Lu, X. Chen and G. Wang, Decorating cobalt phosphide and rhodium on reduced graphene oxide for high-efficiency hydrogen evolution reaction, *J. Energy Chem.*, 2019, **34**, 72–79.

41 B. Qiu, M. Xing and J. Zhang, Recent advances in three-dimensional graphene based materials for catalysis applications, *Chem. Soc. Rev.*, 2018, **47**, 2165–2216.

42 J. Tu, M. Wang, X. Xiao, H. Lei and S. Jiao, Nickel phosphide nanosheets supported on reduced graphene oxide for enhanced aluminum-ion batteries, *ACS Sustain. Chem. Eng.*, 2019, **7**, 6004–6012.

43 H. Wang, Y. Xie, H. Cao, Y. Li, L. Li, Z. Xu, X. Wang, N. Xiong and K. Pan, Flower-Like Nickel Phosphide Microballs Assembled by Nanoplates with Exposed High-Energy (0 0 1) Facets: Efficient Electrocatalyst for the Hydrogen Evolution Reaction, *ChemSusChem*, 2017, **10**, 4899–4908.

44 A. Wu, C. Tian, H. Yan, Y. Jiao, Q. Yan, G. Yang and H. Fu, Hierarchical MoS$_2$@MoP core-shell heterojunction electrocatalysts for efficient hydrogen evolution reaction over a broad pH range, *Nanoscale*, 2016, **8**, 11052–11059.